Ilina, E.; Nyman, M.; Švagždyte, I.; Chekurov, N.; Kaivola, M.; Setälä, T.; Shevchenko, A.

Aberration-insensitive microscopy using optical field-correlation imaging

Published in:
APL Photonics

DOI:
10.1063/1.5091976

Published: 01/06/2019

Document Version
Publisher's PDF, also known as Version of record

APL Photonics

Aberration-insensitive microscopy using optical field-correlation imaging

Cite as: APL Photonics **4**, 066102 (2019); https://doi.org/10.1063/1.5091976
Submitted: 07 February 2019 . Accepted: 28 May 2019 . Published Online: 14 June 2019

E. Ilina, M. Nyman, I. Švagždytė, N. Chekurov, M. Kaivola, T. Setälä, and A. Shevchenko

Aberration-insensitive microscopy using optical field-correlation imaging

Cite as: APL Photon. 4, 066102 (2019); doi: 10.1063/1.5091976
Submitted: 7 February 2019 • Accepted: 28 May 2019 •
Published Online: 14 June 2019

E. Ilina,[1,a)] M. Nyman,[1] I. Švagždytė,[2] N. Chekurov,[3] M. Kaivola,[1] T. Setälä,[4] and A. Shevchenko[1]

AFFILIATIONS

[1] Department of Applied Physics, Aalto University, P.O. Box 13500, FI-00076 Aalto, Finland
[2] Department of Mechanics and Materials Engineering, Vilnius Gediminas Technical University, J. Basanavicius Str. 28, 03224 Vilnius, Lithuania
[3] Oxford Instruments Technologies Oy, Tekniikantie 12, 02650 Espoo, Finland
[4] Institute of Photonics, University of Eastern Finland, P.O. Box 111, FI-80101 Joensuu, Finland

[a)] **Electronic mail:** elena.ilina@aalto.fi

ABSTRACT

The possibility to reduce the effect of optical aberrations has been proposed in several publications on classical ghost imaging. The two-armed ghost-imaging systems make use of spatially incoherent illumination and point-by-point scanned intensity-correlation measurements in the arms. In this work, we introduce a novel ghostlike imaging method that uses a Mach-Zehnder interferometer and is based on optical-field interference instead of intensity correlations. The method allows us to obtain sharp images of microscopic objects even in the presence of severe aberrations that completely destroy the intensity-based image. Furthermore, pure phase objects can be imaged with micrometer-scale resolution in the presence of strong aberrations, which has not been demonstrated previously with a correlation-based imaging technique. In the setup, we use a light-emitting diode source and an ordinary camera as the only light detector. The imaging approach that we put forward in this work may find significant applications in advanced optical microscopy, optical coherence tomography, and a variety of interferometric sensors and detectors.

I. INTRODUCTION

Some optical imaging techniques have been shown to reduce the influence of optical aberrations on the image quality. One of them is optical ghost imaging which is a technique that retrieves images from spatial correlations of optical beams in two arms of an imaging system.[1] Usually, the correlations are obtained either from photon-coincidence or intensity-fluctuation measurements. The illumination is prepared by splitting spatially incoherent light into two beams. One of them propagates through the object to a bucket photodetector with no spatial resolution, while the other one—not interacting with the object—is analyzed pointwise either with a transversely scanned pinhole detector or with a two-dimensional detector array.[2,3] The rate of the detected photon coincidences or the correlations of the intensity fluctuations measured by the detectors in the two arms as a function of the transverse coordinates reveal an object image. Originally, the effect was interpreted as a quantum-mechanical phenomenon in terms of photon entanglement in the two arms.[4] Later, the photon-coincidence detection was replaced with classical intensity-correlation measurements and the same results were obtained.[2,3,5] The intensity fluctuations in the illumination are usually slow as obtained by transmitting a spatially coherent optical beam through a rotating optical diffuser. Hence, the intensity correlations can be measured by considering the correlations of the photocurrents generated by the detectors.[6]

The spatially incoherent illumination required for ghost imaging can also be obtained using thermal light[7] or an amplified-spontaneous-emission (ASE) source,[8] which allows removing the rotating diffuser. However, the associated intensity fluctuations are extremely rapid, necessitating new ultrafast detection methods. One of such approaches—able to assess ultrashort-time scale intensity correlations at reasonably low intensity levels—is based on two-photon absorption in a semiconductor photomultiplier.[8–12] With this technique, however, it is challenging to achieve high-resolution ghost imaging, even with a high-power source.[8] In fact, a large variety of ghost-imaging systems—spreading from the original spatial domain to the time and spectral domains—have been demonstrated using different photodetection methods.[12–15] In all of them, the most intriguing aspect is the capability to reduce the effect of optical aberrations in the object arm,[16–19] which is of interest in the fields of optical microscopy, optical communication and information processing, and in interferometric sensing and detection.[20–23]

Another imaging technique, called full-field optical coherence tomography (FFOCT),[24–28] also uses spatially incoherent illumination. The method is developed for three-dimensional imaging of objects that reflect or backscatter the illuminating light. A typical system is composed of a microscope with an integrated Michelson interferometer in which the object replaces a mirror in one of the arms, and the imaging is based on the field-correlation rather than intensity-correlation measurements. One more crucial difference from ghost imaging is that the light source must have a broad spectrum, thus having a short longitudinal coherence length and giving the system a high longitudinal resolution. Any aberrations in the system should, therefore, not shift the wave fronts of the field by an amount larger than this resolution limit, whose typical value is on the order of 10 μm or smaller.[25–27] Nonetheless, the FFOCT has been demonstrated to successfully reduce the influence of optical aberrations on the image quality.[28] Other techniques also use interference of spatially incoherent light to obtain both amplitude and phase images of transmissive objects. As an example, a type of lensless imaging has been demonstrated using a Mach-Zehnder interferometer with spatially incoherent illumination.[29,30] Furthermore, a single-pixel ghostlike imaging method has been used to image both amplitude and phase objects.[13,31,32] However, the effect of aberrations has not been considered in any of these works. In principle, optical aberrations can be corrected or eliminated by means of adaptive optics[33,34] or by using optical scanning.[35] However, these techniques are not always possible to apply. Furthermore, aberration correction using adaptive optics is problematic in the case of complex and strong aberrations, especially if they are not deterministic. Therefore, scanning-free imaging techniques able to yield sharp images *in the presence* of strong aberrations are of great interest and importance.

In this work, we propose a novel ghostlike imaging system with the following properties. First, similarly to FFOCT microscopes, it uses a spatially incoherent light source, which makes a rotating diffuser unnecessary. Second, a single camera is used, which removes the need to measure photocurrent correlations between two different detectors. Third, spatial correlations of optical fields instead of intensity correlations are measured, which allows imaging of both amplitude and phase objects in the presence of aberrations with a micrometer-scale resolution using standard optical interferometry. In contrast to the FFOCT systems, our method makes use of a Mach-Zehnder interferometer and images light-transmitting objects. Furthermore, while the transverse coherence length of the source is small in our setup, the longitudinal one is large, which makes the system insensitive to even very strong aberrations. As an example, we obtain detailed images of amplitude and phase objects from the interferometric data when the object is screened by an optical diffuser. The imaging approach put forward in this work can be developed toward specific applications in aberration-free microscopy, optical coherence tomography, and various interferometric detector systems that in principle may use both the field and intensity correlations.

II. EXPERIMENTAL SETUP AND EXPLANATION OF THE METHOD

The experimental setup is shown in Fig. 1. The light source is a light-emitting diode (LED) with a 1×1 mm^2 emitting area producing unpolarized and spatially highly incoherent light (M625L3, Thorlabs). Its peak wavelength is 632 nm and the bandwidth is 18 nm. The LED light is collimated by a 10× microscope objective and transmitted through a linear polarizer whose transmission axis can be set to any angle. The polarizer renders the vertical and horizontal electric vector components of the ensuing beam field mutually correlated (as explained below, these components interfere at the camera). A beam splitter divides the beam into two, of which one propagates in the object arm and the other one travels via the reference arm. In the object arm, two 5× microscope objectives with coinciding focal planes are used. The object is inserted in the beam path between the objectives. The first objective creates an image of the LED surface on the object and the second one approximately collimates the field. An identical pair of objectives is inserted in the reference arm at approximately the same distance from the first beam splitter. These objectives flip the image of the LED surface identically in the two arms and enable to tune the wave front curvatures and the transverse positions of the beams in the two arms independently. For more precise tuning, one of the objectives in the reference arm

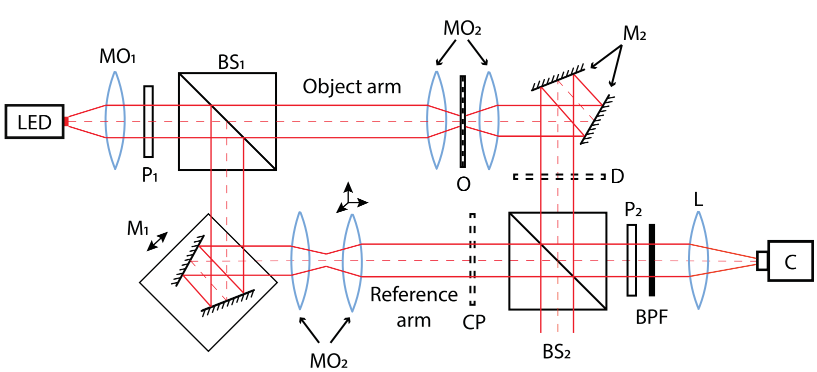

FIG. 1. The experimental setup: MO_1 and MO_2—10× and 5× microscope objectives, respectively; P_1 and P_2—linear polarizers; BS_1 and BS_2—beam splitters; M_1 and M_2—mirrors; O—object; D—diffuser; CP—compensating glass; BPF—bandpass filter; L—lens; C—camera. In the reference arm, the pair of mirrors M_1 can be translated along the direction shown by the arrows, and one of the microscope objectives can be moved in three directions.

is mounted on a 3D translation stage. At the corners of the interferometer's arms, we use two tilted mirrors instead of a single mirror. The mirrors are fixed in position in the object arm, while in the reference arm, they are mounted on a 1D translator. The reference-arm length can be tuned by moving the mirror pair with the translator along the arrow directions marked in Fig. 1. This operation does not change the position nor orientation of the reflected beam. The beams are combined with another beam splitter and transmitted through a linear polarizer. At least one of the beam splitters (preferably BS_1) should be a polarizing beam splitter since then the relative intensities emanating from the arms on the camera can be adjusted by rotating either of the polarizers (preferably P_1). The coherence length of light in the combined beam is increased to ~0.4 mm by letting the beam through a bandpass filter (BPF) of 1 nm bandwidth. The filter can also be placed in front of the LED, but then it is subjected to higher optical power and may be overheated. The camera (acA1920-25uc, Basler) is used with a lens of 100 mm focal length to create a 2.5 times magnified image of the object. The magnification can be easily increased by shifting the sample and the camera, as long as the focal planes of the camera and the objective do not coincide. One can also use a camera lens with a longer focal distance or an objective with a higher magnification.

To introduce aberrations, the image is either defocused or a static optical diffuser is inserted in the object arm in front of the second beam splitter. When the diffuser is used, a compensating glass plate (CP) with a thickness approximately equal to that of the diffuser is used in the reference arm. The interferometric image is obtained by altering the length of the reference arm (which makes the interference fringes on the camera move) and recording a short movie from which the image is retrieved by a computer program that calculates the difference of the maximum and minimum signal values at each pixel. In this way, the time-independent intensity distribution is removed from the image, resulting only in the distribution of intensity variations due to reference arm scanning. It can be shown that the amplitude of the variations is proportional to the modulus of the magnified amplitude-transmittance function of the sample convolved with the modulus of the point-spread function of the imaging system (see the Appendix).

Without aberrations and with the reference arm blocked, the intensity image of the object has a resolution given by the point-spread function of the one-armed system. The numerical aperture of the objective behind the object is $NA = 0.12$. Hence, the resolution is given by $0.6\lambda/NA \approx 3\ \mu$m. In fact, the LED source has a discontinuous emitting surface broken into 10 stripes separated by narrow gaps. To achieve smooth illumination, we first create a sharp image of the emitter in the object plane and then shift the LED back by a distance of $s \approx 1$ mm. The shift defocuses the image of the stripes leading to smoother illumination. Defocusing does not have a significant influence on the measured transverse coherence length of 3 μm, which is also the resolution of the system. When the shift s is large compared to the emitter size L, the increase of the coherence length is approximately given by $\lambda s/L$, which is equal to about 3 μm at $s \approx 5$ mm.[36] When s is smaller or comparable to L, as in our case, the effect of the shift on the coherence length can be neglected.

If both arms are open and aberrations are introduced in the object arm, the resolution of the interferometric image remains unaffected. This can be explained with the help of Fig. 2. Suppose

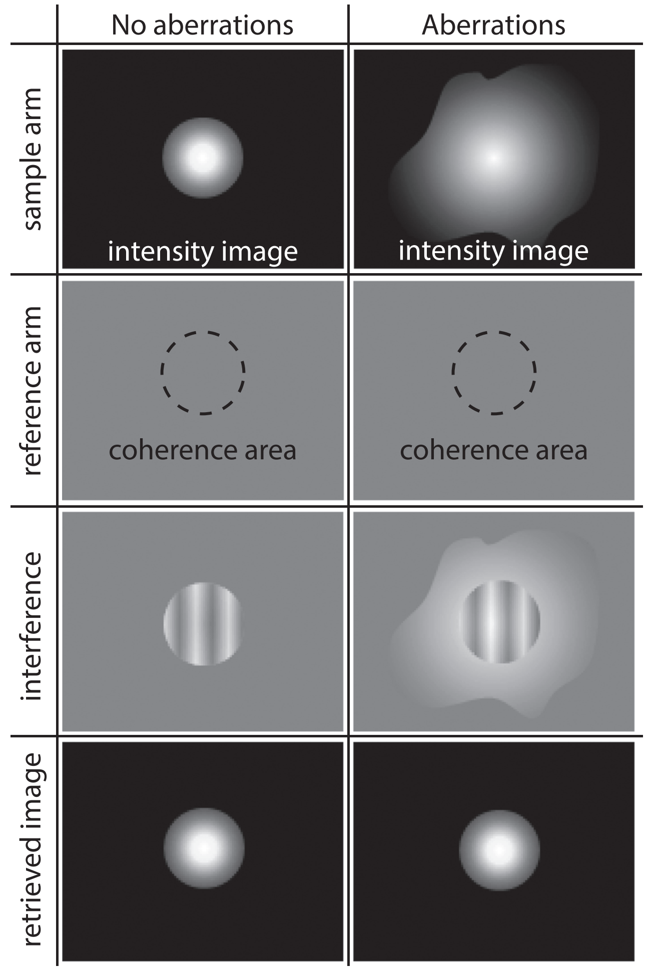

FIG. 2. Schematic of the formation of the interferometric ghostlike image of a pinhole object using the system without and with aberrations in the object arm. The two cases are shown, respectively, in the left and right column. The pictures from top to bottom in each column show (1) the intensity image of the pinhole obtained from the object arm, (2) the coherence area of the reference arm beam in the image plane, (3) the two-arm image, and (4) the retrieved interferometric image.

the object is a pinhole. Without aberrations, its image is a spot determined by the point-spread function (the uppermost picture in the left column). When the reference arm is open, the image is modulated by interference fringes, because a corresponding point in the reference arm produces a spot of the same shape and size as in the object arm (two middle pictures in the left column). Hence, the interferometric image shows the same spot as the object-arm image (the last picture in the left column).

In the presence of aberrations, the intensity image of the pinhole can be large and deformed as shown schematically in the first picture of the right column. However, the corresponding correlating point in the reference arm still produces a diffraction-limited spot. Therefore, interference fringes can be observed only within the area of this spot. Recall that light originating from other points in the reference arm does not correlate with the pinhole light in

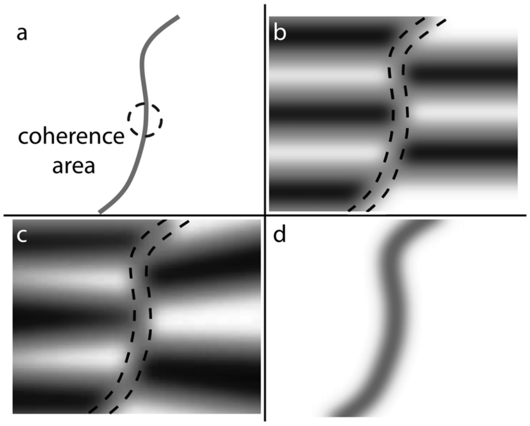

FIG. 3. Schematic of the formation of the interferometric ghostlike image of a sharp edge of a transparent phase object. The edge and the coherence area are shown in (a). The interference fringe patterns in the absence and in the presence of aberrations are shown in (b) and (c), respectively. The retrieved image is shown in (d).

the object arm as long as the illumination is spatially incoherent. Removing from the recorded intensity distribution light that is not modulated by the interference eventually results in the same diffraction-limited pinhole image as obtained without aberrations. Since any amplitude-modulated object can be viewed as a distribution of pinholes, the derived conclusion is valid for any object.[37] For transparent phase objects with abrupt edges, the described technique, independently of aberrations, reveals the edges as described in the Appendix. They are observed in the processed image as dark lines whose width is determined by the point-spread function. This happens due to spatial averaging of the intensity pattern provided by diffraction. As illustrated in Fig. 3, at points close to the phase edge where dark and light interference fringes meet, the averaging (within the area of the point-spread function) effectively reduces the amplitude of the modulated signal. The phase shift at the edges can be evaluated from the shift of the interference fringes. When aberrations are present in the object arm, the fringes are deformed, but they are still shifted at the edges of the object, as illustrated in Fig. 3(c). Thus, the technique reveals the object independently of aberrations.

III. RESULTS

To demonstrate the operation of the system, we fabricated three samples with the logo of Aalto University on them. Two of the logo objects were produced by patterning a film of aluminum on glass with the aid of a laser writer (LW405, MICROTECH). The first logo is formed by metal stripes on glass [see the top picture in Fig. 4(a)] and the second one by slits in the metal film [see the top picture in Fig. 4(b)]. The patterns are therefore negatives of each other. The width of the aluminum stripes in the first sample is 8 μm, while the width of the slits in the second sample is 20 μm. The third sample contains a phase object composed of the Aalto University logo etched in a 1.5 μm thick layer of photoresist on glass [see Figs. 5(a) and 5(b)]. The width of the etched grooves is 24 μm. The photoresist exposure was done using the same laser writer.

Consider first the images of the amplitude-modulated objects presented in Fig. 4. Each column corresponds to one of the samples. The uppermost pictures illustrate the intensity image of the logo when the reference arm is blocked and no aberrations are introduced in the object arm. Hence, the image is sharp. The second picture in each column shows the sample image when aberrations (defocusing or diffuser) are introduced in the object arm. Finally, the lowest picture shows the obtained interferometric ghostlike image which, as characteristics to the technique are revealed with the aid of the reference arm that did not "see" the object at all.

In each set of experiments, the sample blocks part of the incident light power and the aberration leads to an additional power spread decreasing the outcoming object-arm intensity. This reduces the visibility of the interference fringe pattern. To compensate for this change, the beam power incident on the object arm is increased by rotating the linear polarizer P_1 (see Fig. 1) and increasing the source power.

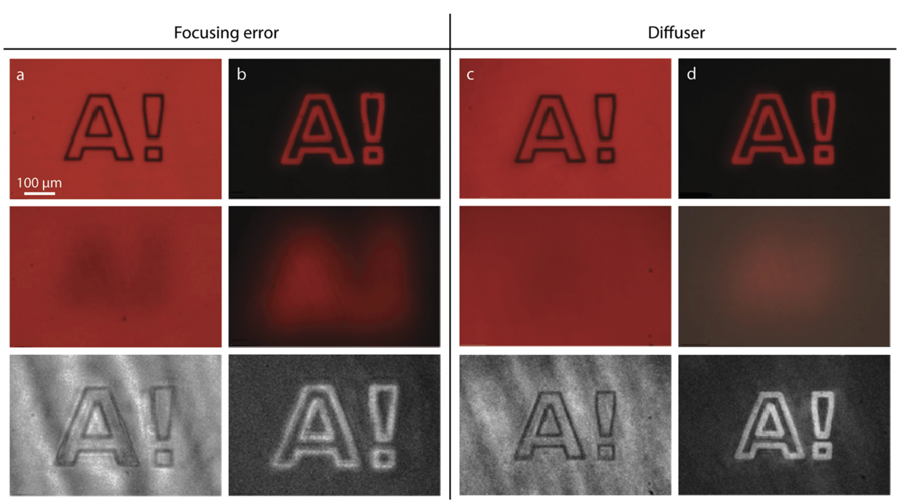

FIG. 4. Optical images of two logos of Aalto University. In the columns, the uppermost and the middle images are, respectively, obtained without and with a focusing error [cases (a) and (b)] or an optical diffuser [cases (c) and (d)] and with the reference arm blocked. The lowermost images are the interferometric images retrieved from the interference patterns of the reference beam and the disturbed object beam.

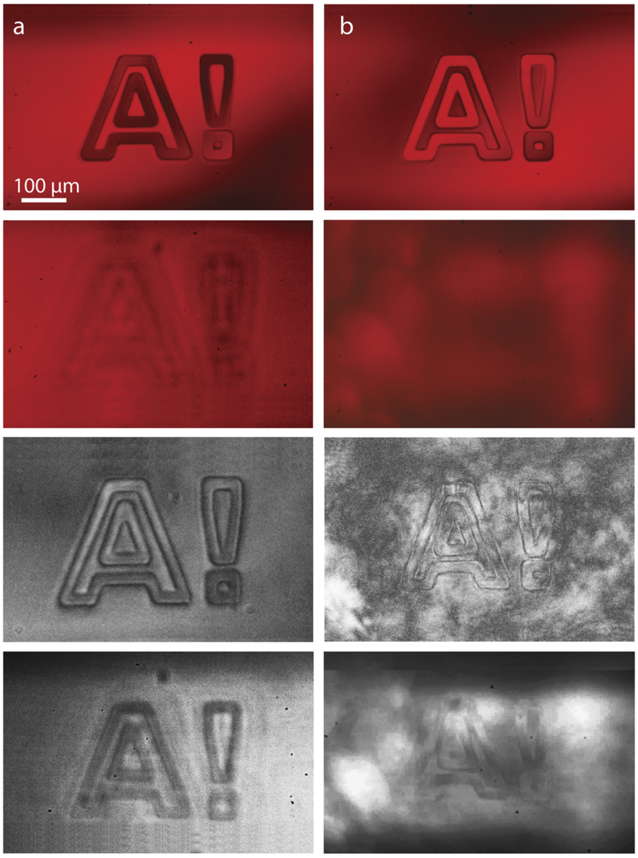

FIG. 5. Optical images of a transparent phase-shifting logo of Aalto University. The logo is an etched pattern in a photoresist film. In both columns, the uppermost image is obtained with the reference arm open in the absence of aberrations. The second image is obtained in the case of a focusing error (left column) or a diffuser (right column). The third image is the retrieved ghostlike image of the sample edges, whereas the lowermost image is an image at a fixed pathlength difference of the arms.

In the experiments concerning the first two columns in Fig. 4, the aberration is a (deterministic) focusing error obtained by displacing the camera by several millimeters along the optical axis. The aberrated intensity images are seen to be severely blurred, although they still give a hint of the objects. The retrieved images, on the other hand, are perfectly sharp. We point out that, in the case of defocusing, the position of the second microscope objective in the reference arm is adjusted such that the transverse coherence area of the reference beam at the image plane is small, which leads to a sharpening of the ghostlike image. It is interesting to note that the shift of the camera increases the magnification of the imaging system even though the object is not shifted. We also see from the images of the two amplitude objects that narrow obstacles are imaged with about the same resolution as narrow openings. The interferometric image of Fig. 4(a) contains a tilted fringe pattern. This pattern is a diffracted image of the defocused emitting stripes of the LED and is not due to the imaging technique itself.

The images in the third and fourth columns of Fig. 4 were obtained with an optical diffuser as a random, nondeterministic aberrating element in the object arm. The aberrations caused by the diffuser are so strong that the objects completely disappear from the images obtained with the object arm alone. However, the retrieved interferometric images are as sharp as the original ones. These results show the striking and exceptional ability of our method to yield sharp ghostlike images of transmissive amplitude-modulated objects in the presence of strong nondeterministic aberrations.

Figure 5 shows the phase-object images in the presence of a focusing error (the left column) and an optical diffuser (the right column). In each column, the uppermost image is obtained without aberrations and with both arms of the setup open so that interference fringes are observed inside and outside the logo. The second picture shows the strongly aberrated intensity image of the object. As before, the logo is nearly completely washed out, especially when applying the diffuser. The third picture shows, in the presence of aberrations, the interferometric image obtained by recording the moving interference fringes and calculating the (temporal) modulation amplitude distribution on the detector array. Both these images show sharp edges of the logo despite the strong aberrations. Finally, the lowermost images illustrate the interference pattern at a fixed pathlength difference of the arms in the presence of aberrations. These patterns can be used to calculate the phase shift imposed by the object on light and the corresponding optical thickness of the object.

IV. CONCLUSION

To summarize, we introduced a single-camera ghostlike imaging microscope based on optical-field interference instead of intensity-correlation measurements. In the system, neither aperture scanning nor interdetector correlation measurements are needed. Compared to intensity-interferometric ghost imaging, the field-interferometric method allows using an ordinary LED with a large emitting area as the required spatially incoherent light source. We demonstrated both theoretically and experimentally that the arrangement is remarkably insensitive to deterministic or nondeterministic optical aberrations. Even by destroying the beam transmitted by the sample with an optical diffuser, perfectly sharp images are obtained from the interferometric data. Furthermore, our technique is able to image microscopic *phase* objects in the presence of strong aberrations. To our knowledge, no other imaging technique has been reported with this ability. The approach can be used also with a spatially intensity-modulated illumination—e.g., to make the correlation time arbitrarily long for even stronger aberrations—and using a Michelson interferometer to image reflective objects. We see a high potential for applications of the method in optical imaging, especially in microscopy of biological and medical samples, as well as for other applications based on optical interferometry. In particular, removing the spectral filter, one can switch the system to a regime of transmissive optical coherence tomography and obtain additional information on the 3D structure of the object.

ACKNOWLEDGMENTS

Part of this research was performed at the Micronova Nanofabrication Center of Aalto University.

This research was funded by the Academy of Finland (Project No. 308394).

APPENDIX: INTERFEROMETRIC IMAGE INTENSITY DISTRIBUTION AND RESOLUTION

The interferometric image intensity distribution and resolution, with and without aberrations, can be calculated within the paraxial approximation using scalar wave optics. In general, if an optical imaging system is characterized by a point-spread function $h(u, v)$, the field $U_i(u, v)$ in the image plane is determined by the convolution integral[38]

$$\begin{aligned} U_i(u,v) &= \int_{-\infty}^{\infty}\int_{-\infty}^{\infty} h(u-x, v-y)U_g(x,y)dxdy \\ &= h(u,v) * U_g(u,v), \end{aligned} \tag{A1}$$

where u and v are the transverse coordinates in the image plane and $U_g(u, v)$ is the geometric-optics image of the object.

Let $U_{go}(u, v)$ be the geometric-optics image of the field incident on the object in the sample arm of Fig. 1 and $U_{go}(u,v)e^{i\phi_{rs}}$ the corresponding field in the reference arm. The phase ϕ_{rs} is the tunable path length phase difference between the arms. Notice that the amplitude $U_{go}(u, v)$ is a random function of time fluctuating independently at each point (u, v) although the time dependence is suppressed for brevity. The object can be characterized by a complex amplitude transmission function whose geometric-optic image is $T_g(u, v)$. In the image plane (detector), the fields from the reference and sample arms are

$$U_r(u,v) = h(u,v) * U_{go}(u,v)e^{i\phi_{rs}}, \tag{A2}$$

$$U_s(u,v) = h_{ab}(u,v) * [T_g(u,v)U_{go}(u,v)], \tag{A3}$$

where $h_{ab}(u, v)$ includes the effect of aberrations. Without aberrations, $h_{ab}(u, v) = h(u, v)$.

The total field in the image plane is $U(u, v) = U_s(u, v) + U_r(u, v)$ and its time-averaged intensity is

$$I(u,v) = \langle |U_s(u,v)|^2\rangle + \langle |U_r(u,v)|^2\rangle + 2\mathrm{Re}\{\langle U_s(u,v)U_r^*(u,v)\rangle\}, \tag{A4}$$

where the angular brackets denote time averaging. Only the third term depends on the path length difference between the arms. The expression $\langle U_s(u,v)U_r^*(u,v)\rangle$ can be written as

$$\begin{aligned} &\langle U_s(u,v)U_r^*(u,v)\rangle \\ &\quad = \langle \int_{-\infty}^{\infty}\int_{-\infty}^{\infty} h_{ab}(u-x,v-y)T_g(x,y)U_{go}(x,y)dxdy \\ &\quad\times \int_{-\infty}^{\infty}\int_{-\infty}^{\infty} h^*(u-\xi,v-\eta)U_{go}^*(\xi,\eta)e^{-i\phi_{rs}}d\xi d\eta\rangle. \end{aligned} \tag{A5}$$

Since only $U_{go}(x, y)$ and $U_{go}(\xi, \eta)$ are time-dependent random functions, we can write

$$\begin{aligned} \langle U_s(u,v)U_r^*(u,v)\rangle &= \int_{-\infty}^{\infty}\int_{-\infty}^{\infty}\int_{-\infty}^{\infty}\int_{-\infty}^{\infty} e^{-i\phi_{rs}}h_{ab}(u-x,v-y) \\ &\quad\times h^*(u-\xi,v-\eta)T_g(x,y)\langle U_{go}(x,y)U_{go}^*(\xi,\eta)\rangle \\ &\quad\times dxdyd\xi d\eta. \end{aligned} \tag{A6}$$

Assuming spatially fully incoherent, constant-intensity $U_{go}(x, y)$, we can replace $\langle U_{go}(x,y)U_{go}^*(\xi,\eta)\rangle$ with the intensity-weighted Dirac delta function $I_{go}\delta(x-\xi, y-\eta)$, leading to

$$\begin{aligned} \langle U_s(u,v)U_r^*(u,v)\rangle &= I_{go}\int_{-\infty}^{\infty}\int_{-\infty}^{\infty} e^{-i\phi_{rs}}h_{ab}(u-x,v-y) \\ &\quad\times h^*(u-x,v-y)T_g(x,y)dxdy. \end{aligned} \tag{A7}$$

The retrieved image intensity profile, $I_{retr}(u, v)$, is obtained by subtracting the minimum value of $I(u, v)$ from its maximum value at each (u, v), when the phase difference ϕ_{rs} of the arms changes at least over 2π. Hence, we obtain

$$\begin{aligned} I_{retr}(u,v) &= 4I_{go}\mathrm{Re}\{\int_{-\infty}^{\infty}\int_{-\infty}^{\infty} h_{ab}(u-x,v-y)h^*(u-x,v-y) \\ &\quad\times |T_g(x,y)|e^{i[\phi_T(x,y)-\phi_{rs}]}dxdy\}|_{max}, \end{aligned} \tag{A8}$$

where max refers to the maximum when the reference-arm length is varied. Notice that at any point (u, v), the variations as a function of ϕ_{rs} are sinusoidal. The phase $\phi_T(x, y)$ is related to $T_g(x, y)$.

Equation (A8) shows that for an amplitude object in the absence of aberrations, the retrieved image intensity is

$$I_{retr}(u,v) \propto |h(u,v)|^2 * |T_g(u,v)|. \tag{A9}$$

In the presence of strong aberrations, the aberrated point-spread function $h_{ab}(u, v)$ is wide compared to $h(u, v)$, and we obtain the following approximate expression:

$$I_{retr}(u,v) \propto |h(u,v)| * |T_g(u,v)|. \tag{A10}$$

If the object is a pinhole, we can model it as $T_g(u, v) = \delta(x, y)$ and obtain

$$I_{retr}(u,v) \propto |h(u,v)|. \tag{A11}$$

For a phase object, we have $T_g(u,v) = e^{i\phi_T(u,v)}$, which leads to a drop of the function $I_{retr}(u, v)$ at the imaged object edges. To show this, let us consider a straight edge that, in the image plane, is parallel to the v-axis and located at $u = 0$. Let the phase shift $\phi_T(u, v)$ be equal to 0 for $u < 0$ and π for $u > 0$. In this case, $T_g(u, v) = 1 - 2H(u)$, where $H(u)$ is the Heaviside step function. It is straightforward to show that, in the absence of aberrations, Eq. (A8) yields

$$I_{retr}(u,v) \propto ||h(u,v)|^2 * [1-2H(u)]|. \tag{A12}$$

The intensity $I_{retr}(u, v)$ smoothly decreases to 0 from both sides when u approaches 0, showing a dark line parallel to the v-axis. The width of the line is determined by the width of $|h(u, v)|^2$. In the presence of strong aberrations, we can as before assume that $h_{ab}(u - x, v - y)$ is wide and find that

$$I_{retr}(u,v) \propto ||h(u,v)| * [1-2H(u)]|. \tag{A13}$$

The width of the line is now larger. We emphasize that if $h_{ab}(u, v)$ is a random function of coordinates u and v, the obtained interferometric image contains random variations of intensity, but the object is still observable through the features described by Eqs. (A10)–(A13).

REFERENCES

[1] B. I. Erkmen and J. H. Shapiro, "Unified theory of ghost imaging with Gaussian-state light," Phys. Rev. A 77, 043809 (2008).
[2] R. S. Bennink, S. J. Bentley, and R. W. Boyd, "'Two-photon' coincidence imaging with a classical source," Phys. Rev. Lett. 89, 113601 (2002).

[3]F. Ferri, D. Magatti, A. Gatti, M. Bache, E. Brambilla, and L. A. Lugiato, "High-resolution ghost image and ghost diffraction experiments with thermal light," Phys. Rev. Lett. **94**, 183602 (2005).
[4]T. B. Pittman, Y. H. Shih, D. V. Strekalov, and A. V. Sergienko, "Optical imaging by means of two-photon quantum entanglement," Phys. Rev. A **52**, R3429–R3432 (1995).
[5]A. Valencia, G. Scarcelli, M. D'Angelo, and Y. Shih, "Two-photon imaging with thermal light," Phys. Rev. Lett. **94**, 063601 (2005).
[6]M. J. Padgett and R. W. Boyd, "An introduction to ghost imaging: Quantum and classical," Philos. Trans. R. Soc., A **375**, 20160233 (2017).
[7]D. Zhang, Y.-H. Zhai, L.-A. Wu, and X.-H. Chen, "Correlated two-photon imaging with true thermal light," Opt. Lett. **30**, 2354–2356 (2005).
[8]S. Hartmann and W. Elsäßer, "A novel semiconductor-based, fully incoherent amplified spontaneous emission light source for ghost imaging," Sci. Rep. **7**, 41866 (2017).
[9]F. Boitier, A. Godard, E. Rosencher, and C. Fabre, "Measuring photon bunching at ultrashort timescale by two-photon absorption in semiconductors," Nat. Phys. **5**, 267 (2009).
[10]A. Shevchenko, M. Roussey, A. T. Friberg, and T. Setälä, "Ultrashort coherence times in partially polarized stationary optical beams measured by two-photon absorption," Opt. Express **23**, 31274–31285 (2015).
[11]A. Shevchenko, M. Roussey, A. T. Friberg, and T. Setälä, "Polarization time of unpolarized light," Optica **4**, 64–70 (2017).
[12]P. Janassek, S. Blumenstein, and W. Elsäßer, "Ghost spectroscopy with classical thermal light emitted by a superluminescent diode," Phys. Rev. Appl. **9**, 021001 (2018).
[13]Y. Bromberg, O. Katz, and Y. Silberberg, "Ghost imaging with a single detector," Phys. Rev. A **79**, 053840 (2009).
[14]P. Ryczkowski, M. Barbier, A. T. Friberg, J. M. Dudley, and G. Genty, "Magnified time-domain ghost imaging," APL Photonics **2**, 046102 (2017).
[15]C. Amiot, P. Ryczkowski, A. T. Friberg, J. M. Dudley, and G. Genty, "Supercontinuum spectral-domain ghost imaging," Opt. Lett. **43**, 5025–5028 (2018).
[16]R. E. Meyers, K. S. Deacon, and Y. Shih, "Turbulence-free ghost imaging," Appl. Phys. Lett. **98**, 111115 (2011).
[17]D. S. Simon and A. V. Sergienko, "Correlated-photon imaging with cancellation of object-induced aberration," J. Opt. Soc. Am. B **28**, 247–252 (2011).
[18]T. Shirai, H. Kellock, T. Setälä, and A. T. Friberg, "Imaging through an aberrating medium with classical ghost diffraction," J. Opt. Soc. Am. A **29**, 1288–1292 (2012).
[19]T. Shirai, "Modern aspects of intensity interferometry with classical light," in *Progress in Optics*, edited by T. D. Visser (Elsevier, 2017), Vol. 62, Chap. 1, pp. 1–72.
[20]W.-K. Yu, X.-R. Yao, X.-F. Liu, R.-M. Lan, L.-A. Wu, G.-J. Zhai, and Q. Zhao, "Compressive microscopic imaging with 'positive-negative' light modulation," Opt. Commun. **371**, 105–111 (2016).
[21]A. Brandenburg, R. Krauter, C. Künzel, M. Stefan, and H. Schulte, "Interferometric sensor for detection of surface-bound bioreactions," Appl. Opt. **39**, 6396–6405 (2000).
[22]S. Chang, X. Liu, X. Cai, and C. P. Grover, "Full-field optical coherence tomography and its application to multiple-layer 2d information retrieving," Opt. Commun. **246**, 579–585 (2005).
[23]Z. Li, J. Suo, X. Hu, and Q. Dai, "Content-adaptive ghost imaging of dynamic scenes," Opt. Express **24**, 7328–7336 (2016).
[24]B. Laude, A. D. Martino, B. Drévillon, L. Benattar, and L. Schwartz, "Full-field optical coherence tomography with thermal light," Appl. Opt. **41**, 6637–6645 (2002).
[25]E. Beaurepaire, A. C. Boccara, M. Lebec, L. Blanchot, and H. Saint-Jalmes, "Full-field optical coherence microscopy," Opt. Lett. **23**, 244–246 (1998).
[26]A. Dubois, K. Grieve, G. Moneron, R. Lecaque, L. Vabre, and C. Boccara, "Ultrahigh-resolution full-field optical coherence tomography," Appl. Opt. **43**, 2874–2883 (2004).
[27]A. Dubois, L. Vabre, A.-C. Boccara, and E. Beaurepaire, "High-resolution full-field optical coherence tomography with a Linnik microscope," Appl. Opt. **41**, 805–812 (2002).
[28]P. Xiao, M. Fink, and A. C. Boccara, "Full-field spatially incoherent illumination interferometry: A spatial resolution almost insensitive to aberrations," Opt. Lett. **41**, 3920–3923 (2016).
[29]S.-H. Zhang, L. Gao, J. Xiong, L.-J. Feng, D.-Z. Cao, and K. Wang, "Spatial interference: From coherent to incoherent," Phys. Rev. Lett. **102**, 073904 (2009).
[30]S.-H. Zhang, S. Gan, D.-Z. Cao, J. Xiong, X. Zhang, and K. Wang, "Phase-reversal diffraction in incoherent light," Phys. Rev. A **80**, 031805 (2009).
[31]P. Clemente, V. Durán, E. Tajahuerce, V. Torres-Company, and J. Lancis, "Single-pixel digital ghost holography," Phys. Rev. A **86**, 041803 (2012).
[32]Y. Liu, J. Suo, Y. Zhang, and Q. Dai, "Single-pixel phase and fluorescence microscope," Opt. Express **26**, 32451–32462 (2018).
[33]M. J. Booth, "Adaptive optical microscopy: The ongoing quest for a perfect image," Light: Sci. Appl. **3**, e165 (2014).
[34]T.-L. Kelly and J. Munch, "Phase-aberration correction with dual liquid-crystal spatial light modulators," Appl. Opt. **37**, 5184–5189 (1998).
[35]Z. Zhang, Z. Su, Q. Deng, J. Ye, J. Peng, and J. Zhong, "Lensless single-pixel imaging by using LCD: Application to small-size and multi-functional scanner," Opt. Express **27**, 3731–3745 (2019).
[36]B. E. A. Saleh and M. C. Teich, *Fundamentals of Photonics*, Wiley Series in Pure and Applied Optics (John Wiley & Sons, New York, 1991).
[37]P. Xiao, M. Fink, A. H. Gandjbakhche, and A. Claude Boccara, "A resolution insensitive to geometrical aberrations by using incoherent illumination and interference imaging," Eur. Phys. J.: Spec. Top. **226**, 1603–1621 (2017).
[38]J. W. Goodman, *Introduction to Fourier Optics* (Roberts and Company Publishers, Englewood, 2005).